Monthly Notices
of the
ROYAL ASTRONOMICAL SOCIETY

MNRAS **499,** 25–39 (2020)
Advance Access publication 2020 September 12

doi:10.1093/mnras/staa2791

Experimental energy levels of $^{12}C^{14}N$ through MARVEL analysis

Anna-Maree Syme and Laura K. McKemmish ★

School of Chemistry, University of New South Wales, 2052 Sydney, Australia

Accepted 2020 August 31. Received 2020 August 23; in original form 2020 July 16

ABSTRACT

The cyano radical (CN) is a key molecule across many different factions of astronomy and chemistry. Accurate, empirical rovibronic energy levels with uncertainties are determined for eight doublet states of CN using the MARVEL (Measured Active Rotational-Vibrational Energy Levels) algorithm. 40 333 transitions were validated from 22 different published sources to generate 8083 spin-rovibronic energy levels. The empirical energy levels obtained from the MARVEL analysis are compared to current energy levels from the MOLLIST line list. The MOLLIST transition frequencies are updated with MARVEL energy level data which brings the frequencies obtained through experimental data up to 77.3 per cent from the original 11.3 per cent, with 92.6 per cent of the transitions with intensities over 10^{-23} cm molecule^{-1} at 1000 K now known from experimental data. At 2000 K, 100.0 per cent of the partition function is recovered using only MARVEL energy levels, while 98.2 per cent is still recovered at 5000 K.

Key words: molecular data – astronomical data bases: miscellaneous – comets: general – planets and satellites: atmospheres – stars: low-mass.

1 INTRODUCTION

The cyano radical (CN) is one of the most important free radicals and is a key molecule in astronomy. CN was one of the first molecules observed in the interstellar medium back in McKellar (1940) and was observed extragalactically in Henkel, Mauersberger & Schilke (1988). Relative to molecular hydrogen, CN has an abundance of around 10^{-9} (Johnstone, Boonman & Van Dishoeck 2003; McElroy et al. 2013) in molecular clouds, which is comparable to other radicals, exceeded mainly by the OH radical. Since its first observation, CN had been also observed in many other astrophysical environments (Schmidt et al. 2013; Sneden et al. 2016; Larsen, Brodie & Strader 2017; McGuire 2018). The cyano free radical is a significant molecule in cometary science (Shinnaka et al. 2017) with its presence and origin not yet completely understood (Fray et al. 2005). Applications of CN in astronomy have included determining the temperature of the cosmic microwave background (Leach 2012), the formation of galaxies (Beckman, Carretero & Vazdekis 2008) and stars (Riffel et al. 2007; Juncher, Jørgensen & Helling 2017) and the abundance of elements (Smith et al. 2013; Ritchey, Federman & Lambert 2015). CN is a principal factor in modelling the growth process of Titan's atmosphere (Woon 2006). The presence of CN is important for determining the isotopic ratios and abundances for both carbon and nitrogen in astrophysical environments (Ritchey et al. 2015; Hamano et al. 2019). With an ionization energy of 112 562.7 cm^{-1}, the CN radical is suggested to have very slow reactions in the cold regions of interstellar media (Gans et al. 2017).

Outside of astronomy, the CN radical is important in chemistry, most notably in high-energy environments such as plasma (Peng et al. 2011), and combustion (Xun, Deng & He 2019), but also for its properties of adsorption on boron nitride nanotubes (Soltani et al. 2013). The CN radical is significant in prebiotic chemistry, as CN is a key intermediate in the production of HCN which is considered central to the origin of life (Woon 2006; Ferus et al. 2017).

Accurately modelling observations of astronomical or other gaseous environments with CN, and thus understanding these environments, requires high accuracy line lists (Smith et al. 2013; Shinnaka et al. 2017; Hamano et al. 2019) – that is, details of all the energy levels in CN and the strength of transitions between these levels. For $^{12}C^{14}N$, the most accurate available data are the MOLLIST line list (Brooke et al. 2014), which considers transitions between the three lowest electronic states of CN, the X $^2\Sigma^+$, A $^2\Pi$, and B $^2\Sigma^+$ states. Full details of how this line list was constructed are deferred until Section 5, but briefly these line list frequencies were computed using the traditional model, that is, fitting experimental transition frequencies to a model Hamiltonian using PGopher to obtain a set of spectroscopic constants which are then used to predict unobserved line frequencies. The MOLLIST traditional model interpolates very accurately but does not extrapolate well because it is based on perturbation theory (Bernath 2020).

In our research, we became interested in CN as a potential probe for testing the variation in the proton-to-electron mass ratio (Syme et al. 2019) based on the near degeneracy of its vibronic levels in the A $^2\Pi$ and X $^2\Sigma^+$ states. However, testing this prediction accurately requires an *ab initio* model of the molecule's spectroscopy, that is, a set of potential energy and coupling curves for which the nuclear motion (vibration-rotation) Schrodinger equation can be solved with slightly different proton masses to determine the sensitivity of different transitions to a variation in the proton-to-electron mass ratio. Lacking this model and given the importance of CN astronomically, we decided to embark on the current paper's goal of collating then validating all available experimental data for CN in

★ E-mail: l.mckemmish@unsw.edu.au

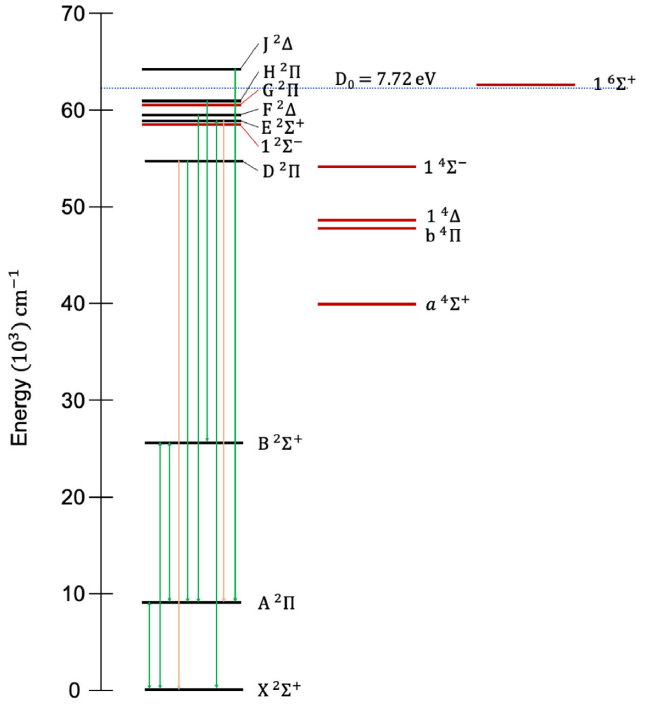

Figure 1. The electronic states and bands in CN. States indicated by the black lines have been experimentally observed. Red lines are electronic states that have been theorized to exist (either by experimental perturbation or theory), but with no available experimental transition data. The vertical green lines indicate electronic bands that have been included in this study, with the orange lines being bands that have been observed, but were not of a suitable nature for this MARVEL procedure. An additional theoretically predicted $1^6\Pi$ state around 96 000 cm^{-1} (Yin et al. 2018) was not included in this figure for brevity. The dissociation energy of CN is shown as a blue dashed line (Pradhan, Partridge & Bauschlicher 1994).

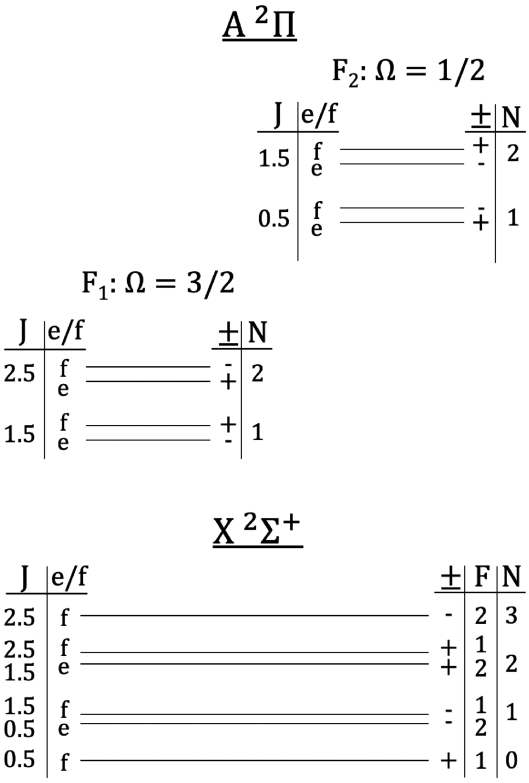

Figure 2. Scheme of quantum number for CN. The quantum numbers (J and e/f) we have used as labels are given on the left-hand side of the lines and the corresponding total parity (±), F (spin multiplet component of the state), and N (angular momentum without the consideration of electron spin) are given on the right-hand side. The spaces between the energy levels are representative only and are not to scale.

a MARVEL (Measured Active Rotational-Vibrational Energy Levels) process, enabling the generation of a full set of experimentally derived energy levels that can be used in the future to create an *ab initio* ExoMol-style line list for CN. A subset of the data we collect here was used to develop the MOLLIST line list, but our work here is a much more extensive compilation that also includes high-lying electronic states not considered in the CN MOLLIST data. This MARVEL compilation will be particularly important for high-resolution studies which rely on very accurate line positions.

Table 1. Sample of the MARVEL input file, with descriptions of the column headings. The full input file is included in the SI.

$\tilde{\nu}$	$\Delta\tilde{\nu}$	Upper state QNs			Lower state QNs			ID
		State$'$	v'	J'	State$''$	v''	J''	
9141.6439	0.012	A2Pi_e1/2	0	0.5	X2Sig+_f	0	0.5	10RaWaBe.19241
25838.0341	0.02	B2Sig+_e	0	9.5	X2Sig+_e	0	8.5	92ReSuMi.8
23748.123	0.03	B2Sig+_f	0	0.5	X2Sig+_f	1	1.5	06RaDaWa.5431
2019.211	0.0008228	X2Sig+_e	1	5.5	X2Sig+_e	0	6.5	05HuCaDa.26
7091.7821	0.012	A2Pi_f1/2	0	0.5	X2Sig+_f	1	1.5	10RaWaBe.17995
5075.763	0.012	A2Pi_f1/2	0	0.5	X2Sig+_f	2	1.5	10RaWaBe.17601
52903.51	0.06	E2Sig+_f	0	0.5	X2Sig+_f	3	1.5	56Ca.383

Column	Notation	
1	$\tilde{\nu}$	Transition frequency (in cm^{-1})
2	$\Delta\tilde{\nu}$	Estimated uncertainty in transition frequency (in cm^{-1})
3	State$'$	Electronic state of upper energy level; also includes parity and Ω for Π and Δ states
4	v'	Vibrational quantum number of upper level
5	J'	Total angular momentum of upper level
6	State$''$	Electronic state of lower energy level; also includes parity and Ω for Π and Δ states
7	v''	Vibrational quantum number of lower level
8	J''	Total angular momentum of lower level
9	ID	Unique ID for transition, with reference key for source and counting number

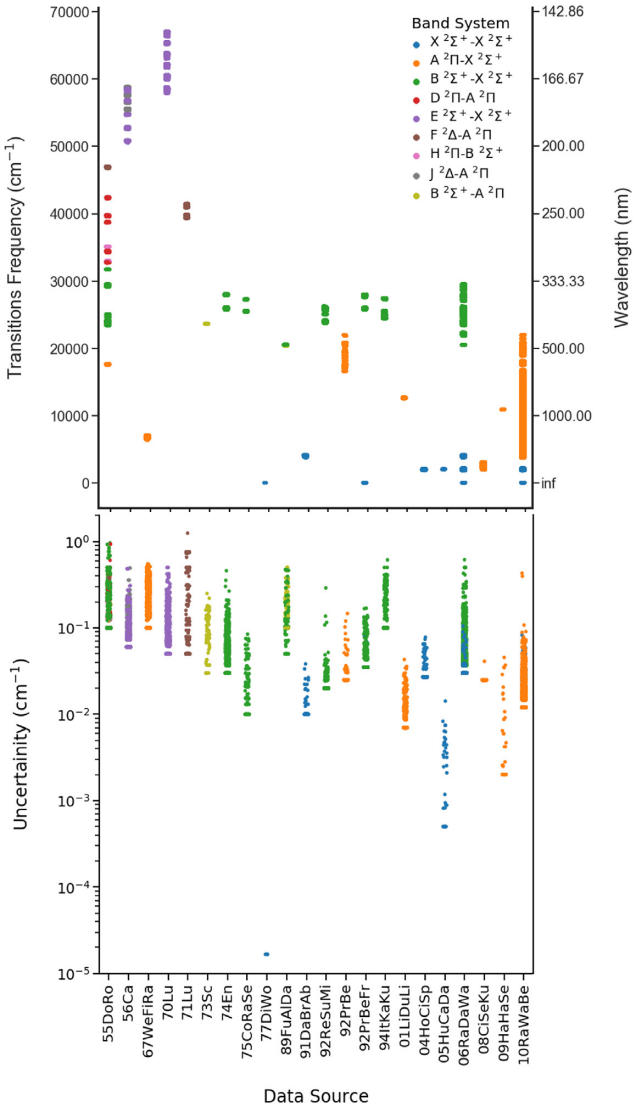

Figure 3. The spread of the frequencies (upper) and uncertainties (lower) of the transitions taken from each data source used in this MARVEL procedure for CN. Each electronic band is shown in a unique colour.

The CN radical is one of the most spectroscopically studied radicals with observations dating back almost 100 yr (Jenkins 1928). Most studies focus on the a combination of the three lowest electronic states (X $^2\Sigma^+$, A $^2\Pi$, and B $^2\Sigma^+$) that contribute to the visible spectroscopic bands. The full electronic states of CN and observed transition bands can be seen in Fig. 1. Below 30 000 cm^{-1}, the electronic structure of CN comprises of a ground state of X $^2\Sigma^+$ followed by the A $^2\Pi$ state around 9145 cm^{-1}, before a larger gap up to the B $^2\Sigma^+$ state around 25 790 cm^{-1}. These lower electronic states contribute to the common CN bands; the red band (A $^2\Pi$-X $^2\Sigma^+$) and the violet band (B $^2\Sigma^+$-A $^2\Pi$), which have been observed many times (Jenkins, Roots & Mulliken 1932; Douglas & Routly 1955; Schoonveld 1973; Schoonyeld & Sundaram 1979; Gorbal & Savadatti 1981; Furio et al. 1989; Prasad & Bernath 1992; Prasad et al. 1992; Rehfuss et al. 1992; Ito, Kazama & Kuchitsu 1994; Liu et al. 2001; Ram et al. 2006; Hause, Hall & Sears 2009; Civiš et al. 2008; Ram, Wallace & Bernath 2010). The B $^2\Sigma^+$-A $^2\Pi$ band is significantly less studied but is an important band in demonstrating that CN could not be treated as a symmetric molecule with u and g symmetry as originally hypothesized (Lutz 1970; Furio et al. 1989). The electronic states above 30 000 cm^{-1} and the associated bands are not as well known. These electronic states are visualized along with the lower electronic states in Fig. 1. Only the doublet states D $^2\Pi$, E $^2\Sigma^+$, F $^2\Delta$, H $^2\Pi$, and J $^2\Delta$ have experimentally assigned transitions from older sources (Douglas & Routly 1955; Carroll 1956; Lutz 1970) however, none of these transitions are doublet resolved. There are several states of the CN radical that have been computationally (Kulik, Steeves & Field 2009; Shi et al. 2011; Yin et al. 2018) or experimentally (Ito et al. 1984) predicted that have no observed transitions. These unobserved states include two possible doublet states around 60 000 cm^{-1}(Lutz 1970; Shi et al. 2011), as well as the quartet and sextet states, and are shown in Fig. 1. The a $^4\Sigma^+$ state is the most established of these unobserved states due to the perturbations it causes in lower electronic states, such as the B $^2\Sigma^+$ state.

The electronic structure of CN might appear at first to be straightforward as the low-lying energy levels are well separated; however, there are strong couplings between states that cause large perturbations affecting many bands. These perturbations have been studied extensively in the 1980s (Kotlar et al. 1980; Gorbal & Savadatti 1982; Ito et al. 1984, 1987, 1994; Ozaki et al.1983a, b) with the Kuchitsu group's many studies on the high vibrational B $^2\Sigma^+$-X $^2\Sigma^+$ bands particularly notable. Near degeneracies of the (A $^2\Pi$ $v = 7$, X $^2\Sigma^+$ $v = 10$) and (B $^2\Sigma^+$ $v = 0$, A $^2\Pi$ $v = 10$) states cause particularly significant perturbations. Further, the high vibrational levels of the B $^2\Sigma^+$ state are rife with perturbations due to coupling to the high vibrational A $^2\Pi$ states and the 'dark' quartet states (Ito et al. 1987, 1984; Ram et al. 2006). These quartet states, shown in Fig. 1 have not been directly observed experimentally, but their properties have been inferred to high precision based on how they perturb observed states (Ito et al. 1984).

The astronomical importance of CN and the substantial perturbations in its spectroscopy have lead to significant *ab initio* investigations into the molecule, with the most accurate calculations being multireference configuration interaction calculations with large basis sets, for example, Bauschlicher, Langhoff & Taylor (1988), Furio et al. (1989), Kulik et al. (2009), Shi et al. (2011), Brooke et al. (2014), and Yin et al. (2018) that cover a range of electronic states. A recent paper (Yin et al. 2018) provides an excellent summary of *ab initio* modelling of CN. In the context of this paper, the most important *ab initio* data to create astronomical line lists are the transition dipole moment (TDM) and spin–orbit coupling curves; the MARVEL experimentally derived energy levels produced in this paper provide a much better data source for creating spectroscopically accurate potential energy curves than *ab initio* data (e.g. see Tennyson et al. 2016; McKemmish et al. 2019). New TDM curves were calculated to enable the production of the (Brooke et al. 2014) line list. Furthermore, in a still rare recognition of the importance for astronomical applications of *ab initio* TDM curves over the more easily calculated but far less useful potential energy curves, we would like to highlight and applaud the recent work from Yin et al. (2018) which expanded the high-accuracy TDM data for CN from the X $^2\Sigma^+$, A $^2\Pi$, and B $^2\Sigma^+$ states to five quartet and two doublet states, though unfortunately other doublet states with energies less than the some of the quartet and sextet states were not included presumably due to the congestion of doublet states around $T_e = 60\,000$ cm^{-1}.

With *ab initio*, newer calculations usually give the best results, but for experimental spectroscopy, the breadth and coverage of data is most important and the complexity of the data means it has been collated over decades. Bringing all this data together in one place in a usable consistent data format, cross-validating the data and extracting

Table 2. Breakdown of the electronic bands of assigned transitions from 20th century sources used in this study. *V* is the number of verified transitions and *A* is the number of available transitions. The mean and maximum uncertainties are given in cm^{-1}, these are after MARVEL has made the transitions self-consistent.

Electronic band	*V*/*A*	Mean/max	Freq range (cm^{-1})	Vibrational bands	*J* range
55DoRo (Douglas & Routly 1955)					
$F\ ^2\Delta$-$A\ ^2\Pi$	58/58	0.142/0.5	46694.9–47062.5	(0-2)	2.5–32.5
$D\ ^2\Pi$-$A\ ^2\Pi$	335/335	0.11/0.931	32662.0–42482.0	(0-6), (0-7), (1-4), (2-4), (3-3)	1.5–27.5
$A\ ^2\Pi$-$X\ ^2\Sigma^+$	106/106	0.104/0.315	17479.4–17664.1	(15-8)	0.5–21.5
$B\ ^2\Sigma^+$-$X\ ^2\Sigma^+$	865/875	0.142/0.961	23344.2–31745.6	(0-1), (1-2), (14-10), (16-13), (18-17), (18-18), (19-15), (19-18), (2-3), (3-4), (4-5), (5-6)	0.5–26.5
$H\ ^2\Pi$-$B\ ^2\Sigma^+$	140/140	0.104/0.249	32878.4–35165.1	(0-0), (0-1),	0.5–17.5
56Ca (Carroll 1956)					
$E\ ^2\Sigma^+$-$X\ ^2\Sigma^+$	529/531	0.089/0.484	50546.9–58595.6	(0-1), (0-2), (0-3), (0-4), (1-1)	0.5–32.5
$J\ ^2\Delta$-$A\ ^2\Pi$	978/986	0.076/0.492	55325.7–58870.7	(0-0), (1-0), (2-0), (3-0)	1.5–30.5
67WeFiRa (Weinberg, Fishburne & Narahari Rao 1967)					
$A\ ^2\Pi$-$X\ ^2\Sigma^+$	377/433	0.228/0.55	6357.4–7107.1	(0-1), (1-2)	3.5–55.5
70Lu (Lutz 1970)					
$E\ ^2\Sigma^+$-$X\ ^2\Sigma^+$	1012/1012	0.083/0.5	57857.7–67093.6	(0-0), (1-0), (1-1), (2-0), (2-1), (3-0), (4-0), (5-0)	0.5–42.5
71Lu (Lutz 1971b)					
$F\ ^2\Delta$-$A\ ^2\Pi$	199/203	0.153/1.247	39306.2–41496.9	(1-6), (1-7), (2-7), (2-8)	0.5–16.5
73Sc (Schoonveld 1973)					
$B\ ^2\Sigma^+$-$A\ ^2\Pi$	70/72	0.099/0.249	23582.6–23708.4	(7-4)	0.5–19.5
74En (Engleman 1974)					
$B\ ^2\Sigma^+$-$X\ ^2\Sigma^+$	1040/1060	0.054/0.458	25743.4–28095.2	(0-0), (1-0), (1-1), (2-1), (2-2), (3-2), (3-3), (4-3), (4-4), (5-4), (5-5), (6-5), (6-6), (7-6), (7-7)	0.5–29.5
75CoRaSe (Coxon, Ramsay & Setser 1975)					
$B\ ^2\Sigma^+$-$X\ ^2\Sigma^+$	128/128	0.025/0.085	25399.1–27322.6	(11-10), (11-11)	1.5–23.5
77DiWo (Dixon & Woods 1977)					
$X\ ^2\Sigma^+$-$X\ ^2\Sigma^+$	4/4	0.0/0.0	3.8–3.8	(1-1), (2-2)	0.5–1.5
89FuAlDa (Furio et al. 1989)					
$B\ ^2\Sigma^+$-$X\ ^2\Sigma^+$	75/77	0.148/0.473	20461.0–20605.0	(8-11)	0.5–21.5
$B\ ^2\Sigma^+$-$A\ ^2\Pi$	94/115	0.198/0.5	20352.0–20543.5	(8-7)	0.5–19.5
91DaBrAb (Davis et al. 1991)					
$X\ ^2\Sigma^+$-$X\ ^2\Sigma^+$	156/156	0.011/0.038	3743.5–4155.4	(2-0)	2.5–57.5
92ReSuMi (Rehfuss et al. 1992)					
$B\ ^2\Sigma^+$-$X\ ^2\Sigma^+$	850/850	0.021/0.29	23720.0–26299.3	(0-0), (0-1), (1-1), (1-2), (11-11), (13-13), (2-2), (2-3), (3-3), (3-4), (4-4), (4-5), (6-6), (6-7), (7-7), (7-8), (8-8), (8-9), (9-10), (9-9)	0.5–63.5
92PrBe (Prasad & Bernath 1992)					
$A\ ^2\Pi$-$X\ ^2\Sigma^+$	266/266	0.028/0.147	16572.9–21982.5	(10-3), (10-4), (11-4), (11-5), (12-4), (12-5), (12-6), (13-5), (13-6), (13-7), (14-5), (14-7), (15-7), (15-8), (16-7), (16-8), (16-9), (19-10), (19-11), (20-10), (20-11), (21-10), (21-11), (8-1), (8-2), (8-3), (9-3)	0.5–6.5
92PrBeFr (Prasad et al. 1992)					
$B\ ^2\Sigma^+$-$X\ ^2\Sigma^+$	720/720	0.041/0.169	25745.3–28025.3	(0-0), (1-0), (1-1), (2-1), (2-2), (3-2), (3-3), (4-3), (4-4), (5-4), (5-5), (6-5), (6-6), (7-6), (7-7), (8-7), (9-8)	0.5–26.5
$X\ ^2\Sigma^+$-$X\ ^2\Sigma^+$	54/54	0.037/0.083	3.5–15.1	(0-0), (1-1), (10-10), (2-2), (3-3), (4-4), (5-5), (6-6), (7-7), (8-8), (9-9)	0.5–3.5
94ItKaKu (Ito et al. 1994)					
$B\ ^2\Sigma^+$-$X\ ^2\Sigma^+$	410/419	0.139/0.612	24383.8–27495.8	(11-11), (14-14), (15-15), (16-14), (18-17), (19-18)	0.5–41.5

meaningful information from the summation of all experimental data is beneficial and useful. Through a series of papers by many authors, this data compilation, cleaning and validation process has been standardised, routinely using the MARVEL software program to convert the collated input assigned transition frequencies with uncertainties into output energy levels with uncertainties, with both input and output files stored online in a single MARVEL website which now contains data for 15 molecules. This centralized data repository and consistent format means that future experiments can easily update existing knowledge with their new data and this data can be easily used to create and update line lists used by astronomers.

Within this paper, we bring together all currently available experimental high-resolution spectra of CN to determine accurate empirical energy levels with reliable uncertainties using the MARVEL approach (Furtenbacher, Császár & Tennyson 2007). In Section 2, we review the MARVEL procedure and the quantum numbers used as labels. The experimental data were prepared in a standardized format, then validated for self-consistency and processed to produce experimentally derived energy levels using the MARVEL procedure. The transition data are discussed in Section 3, while the resultant energy levels are evaluated in Section 4. In Section 5, we compare the MARVEL-derived energy levels with those used in the MOLLIST line

Table 3. Breakdown of the 21st century sources and electronic bands of assigned transitions used for CN.

Electronic band	*V/A*	Mean/max	Freq range (cm^{-1})	Vibrational bands	*J* range
01LiDuLi (Liu et al. 2001)					
$A\,^2\Pi$-$X\,^2\Sigma^+$	189/189	0.013/0.043	12496.8–12735.0	(2-0)	0.5–22.5
04HoCiSp (Horká et al. 2004)					
$X\,^2\Sigma^+$-$X\,^2\Sigma^+$	687/695	0.028/0.078	1816.7–2133.6	(1-0), (2-1), (3-2), (4-3), (5-4), (6-5), (7-6), (8-7)	0.5–31.5
05HuCaDa (Hübner et al. 2005)					
$X\,^2\Sigma^+$-$X\,^2\Sigma^+$	36/36	0.003/0.014	1982.1–2101.3	(1-0)	4.5–17.5
06RaDaWa (Ram et al. 2006)					
$B\,^2\Sigma^+$-$X\,^2\Sigma^+$	5775/5801	0.036/0.614	20441.5–29549.9	(0-0), (0-1), (1-0), (1-1), (1-2), (10-10), (10-11), (10-12), (10-8), (10-9), (11-10), (11-11), (11-12), (11-13), (11-9), (12-10), (12-11), (12-12), (12-13), (12-14), (13-11), (13-13), (14-14), (15-15), (16-13), (17-14), (17-16), (18-17), (18-18), (19-15), (19-18), (2-1), (2-2), (2-3), (3-2), (3-3), (3-4), (4-3), (4-4), (4-5), (4-6), (5-4), (5-5), (5-6), (5-7), (6-5), (6-6), (6-7), (6-8), (7-10), (7-6), (7-7), (7-8), (7-9), (8-10), (8-7), (8-8), (8-9), (9-10), (9-11), (9-12), (9-7), (9-8), (9-9)	0.5–63.5
$X\,^2\Sigma^+$-$X\,^2\Sigma^+$	1788/1788	0.031/0.105	3.5–4155.4	(0-0), (1-0), (1-1), (10-10), (2-0), (2-1), (2-2), (3-1), (3-2), (3-3), (4-2), (4-3), (4-4), (5-4), (5-5), (6-5), (6-6), (7-6), (7-7), (8-7), (8-8), (9-9)	0.5–79.5
08CiSeKu (Civiš et al. 2008)					
$A\,^2\Pi$-$X\,^2\Sigma^+$	870/870	0.025/0.041	1905.8–3117.2	(0-3), (1-4), (2-5), (3-6), (4-7), (5-8), (6-9)	1.5–31.5
09HaHaSe (Hause et al. 2009)					
$A\,^2\Pi$-$X\,^2\Sigma^+$	38/38	0.009/0.045	10850.0–10937.3	(1-0)	0.5–7.5
10RaWaBe (Ram et al. 2010)					
$A\,^2\Pi$-$X\,^2\Sigma^+$	20695/20707	0.013/0.429	3683.4–22027.6	(0-0), (0-1), (0-2), (1-0), (1-1), (1-2), (1-3), (10-5), (10-6), (11-6), (12-7), (13-7), (14-6), (14-7), (15-7), (15-8), (16-7), (16-8), (17-10), (17-8), (18-10), (18-9), (19-10), (19-11), (2-0), (2-1), (2-2), (2-3), (2-4), (20-10), (21-10), (21-11), (22-11), (22-12), (3-0), (3-1), (3-2), (3-3), (3-4), (3-5), (4-0), (4-1), (4-2), (4-4), (4-5), (4-6), (5-1), (5-2), (5-3), (5-5), (5-7), (6-2), (6-3), (6-4), (6-6), (6-7), (6-8), (7-7), (7-8), (8-3), (8-4), (8-9), (9-4)	0.5–113.5
$X\,^2\Sigma^+$-$X\,^2\Sigma^+$	1786/1788	0.013/0.083	3.5–4155.4	(0-0), (1-0), (1-1), (10-10), (2-0), (2-1), (2-2), (3-1), (3-2), (3-3), (4-2), (4-3), (4-4), (5-4), (5-5), (6-5), (6-6), (7-6), (7-7), (8-7), (8-8), (9-9)	0.5–79.5

list, and improve the current line list by MARVELizing the MOLLIST states file.

2 MARVEL PROCEDURE FOR CN

The MARVEL approach (Furtenbacher et al. 2007) uses an algorithm to invert experimentally assigned transitions to empirical rovibrationic energy levels. The MARVEL procedure uses graph theory, creating spectroscopic networks (SN, Császár & Furtenbacher 2011) containing all connected energy levels from the experimental transitions. Uncertainties of assigned transitions are adjusted with a weighted strategy until self-consistent. These uncertainties are then propagated through to the associated energy levels to provide reliable energy level uncertainties.

The MARVEL procedure has been documented many times (Furtenbacher et al. 2007, 2013a,b, 2014; Furtenbacher & Császár 2012) and we refer the reader to the original papers for further details. The MARVEL procedure is well established (e.g. see Furtenbacher et al. 2013a,b, 2016, 2019; McKemmish et al. 2017, 2018) and has been used to determine the empirical energy levels of 15 small molecules and their isotopologues. MARVEL analysis of small molecules has been used to compute accurate, temperature-dependent ideal-gas thermodynamic data (e.g. Furtenbacher et al. 2019), to facilitate the empirical adjustment of potential energy surfaces (e.g. Yurchenko et al. 2018), and to improve the accuracy of computed line lists (e.g. McKemmish et al. 2019). The online user interface of MARVEL was used for this work and is available at http://kkrk.chem.elte.hu/marvelonline/.

2.1 *Quantum numbers*

The MARVEL procedure relies solely on labelling of quantum states. The quantum states are treated as nodes connected by transitions as directed edges in a graph and do not have any physics built in, for example, model Hamiltonians.

For our MARVEL CN compilation, each quantum state is described uniquely by a set of three quantum numbers: the State, the vibrational quantum number v, and the total angular momentum J, as shown in the input file extract in Table 1. The last two are straightforward, with the only note being that we chose to use Hund's case A labelling J not N (the rotational-only angular momentum) for consistency with most sources and the MOLLIST line list. The State label, however, is more complicated as it includes not only the electronic state but also the spin splitting through the explicit inclusion of *e/f* rotational-less

Table 4. Sources considered but not used in the MARVEL procedure, with comments for justification.

Reference	Comments
Jenkins (1928)	Very early source with a lot of blended lines, more recent sources cover all the reported bands at higher resolution.
Jenkins et al. (1932)	Misassigned bands, unclear which they should be
Irwin & Dalby (1965)	Computation of dipole moments and transition probabilities
Poletto & Rigutti (1965)	Vibrational and rotational constants
Leblanc (1968)	Only band heads
Schoonveld (1972)	Franck–Condon factors
Phillips & Chun (1973)	Band heads
Cerny et al. (1978)	Analyses rotationally resolved data, later considered by 10RaWaBe, but does not contain the raw experimental assigned transitions in a form suitable for MARVEL analysis
Duric, Erman & Larsson (1978)	Lifetimes
Schoonyeld & Sundaram (1979)	Outdated data, higher resolution of same bands covered by 06RaDaWa (Ram et al. 2006)
Kotlar et al. (1980)	Coupling, no assigned spectra, perturbations
Gorbal & Savadatti (1981)	Significantly different assignments to bands from more recent publications, very small change to main SN when included.
Ito et al. (1984)	No assigned spectra
Ito et al. (1988)	Coupling, no assigned spectra
Ajitha & Hirao (2001)	Calculated dipole moments for X and A
Shi et al. (2010)	Constants, no assigned spectra
Shi et al. (2011)	Computation of PEC for eight low-lying states
Colin & Bernath (2012)	Isotopologue data for $^{12}C^{15}N$
Ram & Bernath (2012)	Isotopologue data for $^{13}C^{14}N$
Brooke et al. (2014)	Line list creation, calculation of TDM and lifetimes
Colin & Bernath (2014)	Isotopologue data for $^{13}C^{15}N$
Sneden et al. (2014)	Line list for isotopologues
Wasowicz et al. (2014)	No rotationally resolved assignments
Ferus et al. (2017)	No assigned spectra published
Qin, Zhao & Liu (2017)	Computational
Yin et al. (2018)	Computational

parity and Ω labels when the quantum states were not degenerate. Fig. 2 shows an example of the labelling used for a selection of the energy levels in the $X\,^2\Sigma^+$ and $A\,^2\Pi$ states, with both our quantum numbers and other commonly used quantum numbers included for clarity.

3 EXPERIMENTAL SOURCES FOR ASSIGNED TRANSITIONS

3.1 Overview

An extensive literature search was done to find, to our knowledge, an exhaustive list of experimentally assigned rotationally resolved transitions for CN. 22 published sources were identified as containing assigned transitions suitable for the MARVEL procedure here. Throughout the literature search, no new experimental assignments were found post 2010 and the higher electronic band have been significantly less studied, with no viable high-resolution data since the 1970s.

The complete transitions input file to MARVEL (a sample is shown in Table 1) consists of 40 333 assigned transitions, from nine electronic bands and is included in the Supporting Information.

To obtain this file, the following procedure was followed. The rotationally resolved assigned transitions data for each source was converted to MARVEL format, with each transition given a starting uncertainty based on discussion in the original paper. This process was not straightforward in many cases, so we give individual notes on each source in Section 3.2. The MARVEL procedure was then used to check for self-consistency within the source's assigned transitions, with uncertainties increased and some transitions with very large uncertainties removed until self-consistency was obtained. Then, the MARVEL data for each individual source were sequentially put into a single master MARVEL file, with uncertainties then adjusted and further transitions removed until self-consistency of the full file was obtained. Note that the transitions removed are retained in the file itself but with a '-' at the beginning of the file to indicate it is not part of the SN obtained by the MARVEL procedure for the molecule. We refer to the remaining transitions as verified.

The spectroscopic data from the 22 sources and results from the MARVEL analysis are summarized in Fig. 3 and detailed in Tables 2 and 3.

Fig. 3 shows the frequency coverage of spectral data below 30 000 cm^{-1} is quite exhaustive due primarily to 06RaDaWa (Ram et al. 2006) and 10RaWaBe (Ram et al. 2010), but is sparser at higher frequencies. Both 06RaDaWa and 10RaWaBe focus on a comprehensive global fit of a single band ($B\,^2\Sigma^+$-$X\,^2\Sigma^+$ and $A\,^2\Pi$-$X\,^2\Sigma^+$, respectively) and equilibrium spectroscopic constants, performing new analysis of existing but unpublished experimental data. The MARVEL approach in this paper provides a different, complementary perspective on this data by using graph theory rather than model Hamiltonian fits.

Table 5. Sample of the MARVEL output energies file. The full output file is included in the SI.

State	v	J	E	ΔE	#
X2Sig+_e	3	5.5	6103.507576	0.001771	89
A2Pi_e3/2	0	4.5	9129.091256	0.002998	27
X2Sig+_e	8	8.5	15726.855299	0.002278	55
A2Pi_e3/2	5	7.5	17871.555021	0.003399	14
X2Sig+_e	8	10.5	15793.319748	0.002338	53
A2Pi_e3/2	5	9.5	17928.336351	0.003156	16

Column	Notation	
1	State	Electronic state of the energy level; also includes parity and Ω for Π and Δ states
2	v	Vibrational quantum number of the state
3	J	Total angular momentum of the state
4	E	Energy in cm^{-1} of the state
5	ΔE	Uncertainty in cm^{-1} of the state
6	#	Number of transitions from the input file that contribute to the energy of the state

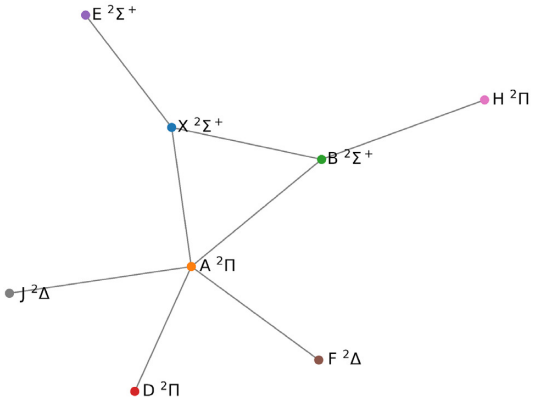

(a) Network of electronic states.

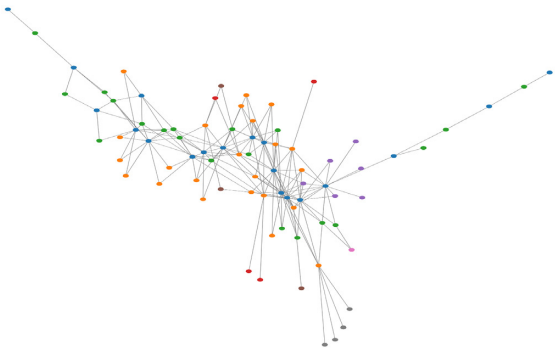

(b) Network of vibronic states of CN.

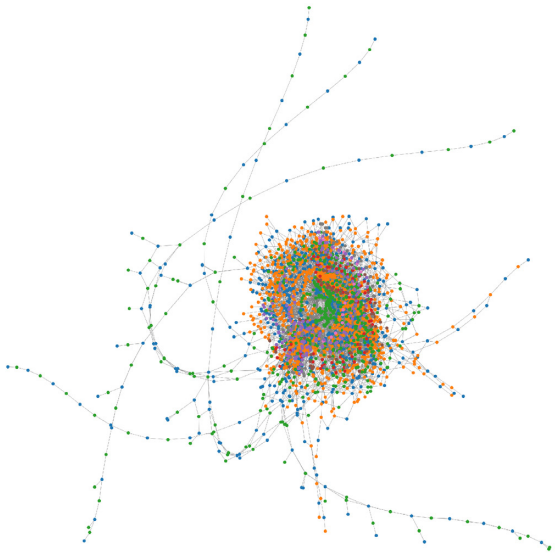

(c) Main Spectroscopic Network of rovibronic states.

Figure 4. SN of CN produced using the MARVEL input and output data. The energy levels are displayed as nodes and the transitions are the edges that join the nodes. Each electronic state is given a colour which is labelled in subfigure (a) and repeated in subfigures (b) and (c).

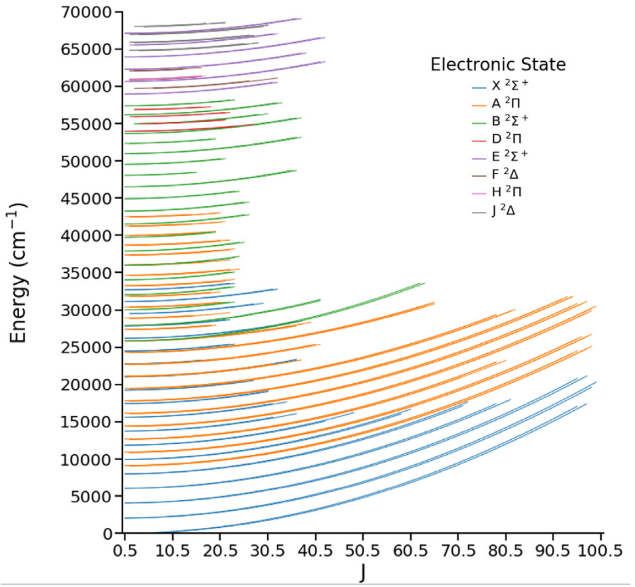

Figure 5. The spin-vibronic energy levels as a function of the total angular momentum, J. Each colour is the electronic state that the energy level belongs to.

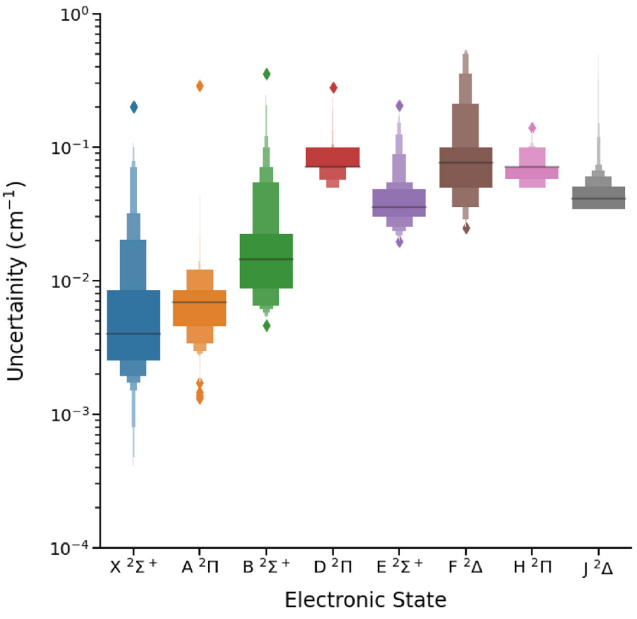

Figure 6. The spread of uncertainties for each electronic state in CN. The solid line across the largest box shows the mean uncertainty, with the diamond points indicating the highest and lowest values for each electronic state.

The lower part of Fig. 3 highlights the spread of uncertainties for each source that are produced through the MARVEL procedure. This figure is slightly skewed by the incredibly small uncertainty of the hyperfine transitions from 77DiWo (Dixon & Woods 1977). Besides the outlier of 77DiWo, most of the data sources from before the 1990s have a much higher starting uncertainty, however, the spread of uncertainties is much the same as we go through more modern assignments. From the transitions between the lower electronic states, we can see in Fig. 3 that the B $^2\Sigma^+$-X $^2\Sigma^+$ band system generally has a higher uncertainty. This heightened uncertainty is possibly due to its position in the ultraviolet region, or the numerous instances of other states perturbing the B $^2\Sigma^+$-X $^2\Sigma^+$ band.

Tables 2 and 3 consider sources from the 20th and 21st century respectively and detail not only the original data (i.e. band, number of assigned transitions, vibrational bands, J range, and frequency range) but also the results of the MARVEL procedure (number of validated

Table 6. Summary of experimentally derived MARVEL energy levels, including uncertainties and data sources, for low-lying electronic states of CN. No is the number of energy levels in that vibronic state.

v	J range	E-range (cm^{-1})	No	Mean/max	Sources
$X^2\Sigma^+$					
0	0.5–97.5	0.0–17403.4	194	0.003/0.005	06RaDaWa, 10RaWaBe, 92PrBeFr, 01LiDuLi, 04HoCiSp, 05HuCaDa, 09HaHaSe, 70Lu, 74En, 91DaBrAb, 92ReSuMi
1	0.5–99.5	2042.4–20317.7	195	0.003/0.008	04HoCiSp, 05HuCaDa, 06RaDaWa, 10RaWaBe, 77DiWo, 92PrBeFr, 55DoRo, 56Ca, 67WeFiRa, 70Lu, 74En, 92PrBe, 92ReSuMi
2	0.5–97.5	4058.5–21127.9	194	0.003/0.008	04HoCiSp, 06RaDaWa, 10RaWaBe, 77DiWo, 91DaBrAb, 92PrBeFr, 55DoRo, 56Ca, 67WeFiRa, 74En, 92PrBe, 92ReSuMi
3	0.5–81.5	6048.3–17978.5	161	0.003/0.008	04HoCiSp, 06RaDaWa, 10RaWaBe, 92PrBeFr, 08CiSeKu, 55DoRo, 56Ca, 74En, 92PrBe, 92ReSuMi
4	0.5–72.5	8011.8–17661.4	145	0.004/0.012	04HoCiSp, 06RaDaWa, 10RaWaBe, 92PrBeFr, 08CiSeKu, 55DoRo, 56Ca, 74En, 92PrBe, 92ReSuMi
5	0.5–60.5	9948.8–16676.8	117	0.005/0.012	04HoCiSp, 06RaDaWa, 10RaWaBe, 92PrBeFr, 08CiSeKu, 55DoRo, 74En, 92PrBe, 92ReSuMi
6	0.5–48.5	11859.3–16195.3	92	0.005/0.012	04HoCiSp, 06RaDaWa, 10RaWaBe, 92PrBeFr, 08CiSeKu, 55DoRo, 74En, 92PrBe, 92ReSuMi
7	0.5–36.5	13743.4–16086.8	69	0.003/0.008	04HoCiSp, 06RaDaWa, 10RaWaBe, 92PrBeFr, 08CiSeKu, 74En, 92PrBe, 92ReSuMi
8	0.5–34.5	15600.9–17674.3	67	0.004/0.012	04HoCiSp, 06RaDaWa, 10RaWaBe, 92PrBeFr, 08CiSeKu, 55DoRo, 92PrBe, 92ReSuMi
9	0.5–30.5	17431.8–19143.5	62	0.005/0.012	06RaDaWa, 10RaWaBe, 92PrBeFr, 08CiSeKu, 92PrBe, 92ReSuMi
10	0.5–27.5	19236.0–20528.0	54	0.007/0.03	06RaDaWa, 10RaWaBe, 92PrBeFr, 55DoRo, 75CoRaSe, 92PrBe, 92ReSuMi
11	0.5–36.5	21013.3–23384.8	74	0.029/0.1	06RaDaWa, 10RaWaBe, 75CoRaSe, 89FuAlDa, 92PrBe, 92ReSuMi, 94ItKaKu
12	0.5–19.5	22765.7–23402.5	37	0.007/0.03	06RaDaWa, 10RaWaBe
13	0.5–23.5	24488.7–25403.2	47	0.016/0.064	06RaDaWa, 55DoRo, 92ReSuMi
14	0.5–37.5	26185.7–28479.7	75	0.04/0.201	06RaDaWa, 94ItKaKu
15	0.5–22.5	27856.2–28676.2	45	0.034/0.1	06RaDaWa, 55DoRo, 94ItKaKu
16	1.5–29.5	29502.0–30889.3	54	0.045/0.133	06RaDaWa
17	0.5–32.5	31115.1–32784.5	64	0.04/0.1	06RaDaWa, 55DoRo, 94ItKaKu
18	0.5–23.5	32703.8–33566.9	47	0.027/0.1	06RaDaWa, 55DoRo, 94ItKaKu
$A^2\Pi$					
0	0.5–98.5	9094.3–25099.4	385	0.004/0.012	08CiSeKu, 10RaWaBe, 67WeFiRa, 56Ca
1	0.5–98.5	10882.0–26718.0	387	0.006/0.012	08CiSeKu, 09HaHaSe, 10RaWaBe, 67WeFiRa
2	0.5–80.5	12644.2–23241.4	306	0.006/0.012	01LiDuLi, 08CiSeKu, 10RaWaBe, 55DoRo
3	0.5–99.5	14380.7–30495.4	377	0.006/0.02	08CiSeKu, 10RaWaBe, 55DoRo
4	0.5–97.5	16091.7–31122.4	360	0.008/0.014	08CiSeKu, 10RaWaBe, 55DoRo, 73Sc
5	0.5–94.5	17777.1–31777.3	326	0.008/0.025	08CiSeKu, 10RaWaBe
6	0.5–82.5	19436.8–30073.8	298	0.008/0.02	08CiSeKu, 10RaWaBe, 55DoRo, 71Lu
7	0.5–37.5	21070.9–23301.8	136	0.008/0.1	10RaWaBe, 55DoRo, 71Lu, 89FuAlDa
8	0.5–41.5	22679.3–25386.9	147	0.007/0.04	10RaWaBe, 92PrBe, 71Lu
9	0.5–65.5	24262.0–31016.2	219	0.009/0.024	10RaWaBe, 92PrBe
10	0.5–39.5	25818.9–28341.6	146	0.008/0.012	10RaWaBe, 92PrBe
11	0.5–19.5	27350.0–27956.4	73	0.01/0.012	10RaWaBe, 92PrBe
12	0.5–22.5	28855.1–29622.4	60	0.01/0.013	10RaWaBe, 92PrBe
13	0.5–21.5	30334.4–31047.1	76	0.011/0.012	10RaWaBe, 92PrBe
14	0.5–20.5	31787.5–32410.5	70	0.009/0.012	10RaWaBe, 92PrBe
15	0.5–23.5	33214.4–34107.2	86	0.011/0.1	10RaWaBe, 55DoRo, 92PrBe
16	0.5–24.5	34615.0–35478.6	83	0.008/0.012	10RaWaBe, 92PrBe
17	0.5–22.5	35988.9–36709.4	68	0.009/0.042	10RaWaBe
18	0.5–23.5	37336.3–38195.2	85	0.008/0.018	10RaWaBe
19	0.5–22.5	38656.7–39357.8	80	0.013/0.291	10RaWaBe, 92PrBe
20	0.5–19.5	39949.8–40545.7	66	0.011/0.018	10RaWaBe, 92PrBe
21	0.5–21.5	41215.4–41837.7	66	0.009/0.048	10RaWaBe, 92PrBe
22	0.5–20.5	42453.0–43011.2	66	0.009/0.02	10RaWaBe
$B^2\Sigma^+$					
0	0.5–63.5	25797.9–33588.7	114	0.012/0.045	06RaDaWa, 55DoRo, 74En, 92PrBeFr, 92ReSuMi
1	0.5–41.5	27921.5–31399.2	65	0.013/0.04	06RaDaWa, 55DoRo, 74En, 92PrBeFr, 92ReSuMi
2	0.5–23.5	30004.9–31060.8	46	0.012/0.036	06RaDaWa, 55DoRo, 74En, 92PrBeFr, 92ReSuMi
3	0.5–23.5	32045.9–33095.6	47	0.012/0.03	06RaDaWa, 55DoRo, 74En, 92PrBeFr, 92ReSuMi
4	0.5–23.5	34042.0–35072.4	47	0.011/0.029	06RaDaWa, 55DoRo, 74En, 92PrBeFr, 92ReSuMi
5	0.5–24.5	35990.0–37186.5	48	0.014/0.067	06RaDaWa, 55DoRo, 74En, 92PrBeFr
6	0.5–25.5	37887.4–39066.8	51	0.013/0.03	06RaDaWa, 74En, 92PrBeFr, 92ReSuMi
7	0.5–19.5	39730.5–40409.0	39	0.01/0.041	06RaDaWa, 73Sc, 74En, 92PrBeFr, 92ReSuMi
8	0.5–26.5	41516.6–42749.5	50	0.012/0.03	06RaDaWa, 89FuAlDa, 92PrBeFr, 92ReSuMi

Table 6 – *continued*

v	J range	E-range (cm^{-1})	No	Mean/max	Sources
9	0.5–26.5	43243.0–44452.5	53	0.009/0.02	06RaDaWa, 92PrBeFr, 92ReSuMi
10	0.5–24.5	44908.8–45924.5	49	0.014/0.03	06RaDaWa
11	0.5–36.5	46511.4–48708.3	73	0.03/0.1	06RaDaWa, 75CoRaSe, 92ReSuMi, 94ItKaKu
12	0.5–15.5	48053.7–48443.6	31	0.009/0.014	06RaDaWa
13	0.5–21.5	49537.3–50273.5	43	0.016/0.03	06RaDaWa, 92ReSuMi
14	0.5–37.5	50967.7–53146.3	71	0.073/0.354	06RaDaWa, 55DoRo, 94ItKaKu
15	0.5–19.5	52343.0–52921.1	38	0.038/0.1	06RaDaWa, 94ItKaKu
16	0.5–37.5	53664.4–55753.6	75	0.069/0.259	06RaDaWa, 55DoRo, 94ItKaKu
17	2.5–30.5	54955.1–56299.8	54	0.026/0.077	06RaDaWa
18	0.5–33.5	56178.1–57782.9	64	0.036/0.1	06RaDaWa, 55DoRo, 94ItKaKu
19	0.5–23.5	57371.3–58145.5	47	0.041/0.089	06RaDaWa, 55DoRo, 94ItKaKu

transitions, mean and maximum uncertainties for the processed data). Vibronic-resolution versions of these tables are provided in the Supporting Information. Many sources had a small number of unverified transitions due to misassignments and large uncertainties, but none are concerning. Similarly, the maximum uncertainty was always within an order of magnitude of the mean uncertainty, indicating there were no significant problems in the data.

Some papers were found with CN spectroscopic data that were not suitable for our compilation; these are listed in Table 4 with justifications for their exclusion.

3.2 Individual source notes

Many papers give uncertainties that we adopt unaltered and found to be reasonably consistent with all other CN data.

Several sources (Douglas & Routly 1955; Carroll 1956; Lutz 1970, 1971b; Engleman 1974; Furio et al. 1989; Davis et al. 1991; Prasad et al. 1992; Ito et al. 1994; Hübner et al. 2005) considering Σ–Σ transitions did not resolve the doublet splitting at low J. We addressed this by including the two unresolved transitions as separate assigned transitions with the same frequency in the MARVEL compilation.

Further comments on individual sources are:

55DoRo (Douglas & Routly 1955)

The D $^2\Pi$-X $^2\Sigma^+$ band was not included due to a lack of labelling of the spin splitting (Ω) of the D $^2\Pi$ state, as such we were unable to assign reliable quantum numbers. A higher leeway in uncertainties was given for the higher electronic states. Transitions were excluded from the MARVEL procedure if the MARVEL uncertainty grew to be greater than 1 cm^{-1}.

67WeFiRa (Weinberg et al. 1967)

Several lines needed to be shifted to become self-consistent; 0–1 R(11)(35) was increased 100 cm^{-1}, 0–1 Q(11)(24) decreased 10 cm^{-1}, 1–2 P(11)(38) increased 10 cm^{-1}, and 1–2 P(22)(25) decreased 5 cm^{-1}. When adding to the bulk of the transitions several lines were deleted due to increased uncertainty, this was deemed acceptable as there were no new energy levels involved, so newer data took precedent.

70Lu (Lutz 1970)

Only a few transitions had doublet structure recorded, but with no clear assignment of quantum numbers, these transitions were averaged. The transition in the E $^2\Sigma^+$-X $^2\Sigma^+$ (3−0) band at N= 26 was changed from 809.43 to 689.43 to ensure consistency.

71Lu (Lutz 1971b)

No assigned uncertainty within this paper due to the experimental details being published in a previous work on CN^+ (Lutz 1971a), thus we have taken the relative uncertainty from there.

73Sc (Schoonveld 1973)

One of only two sources with rotationally resolved transitions of the B $^2\Sigma^+$-A $^2\Pi$ band. Internally self-consistent, but two transitions were removed when ensuring self consistency with the rest of the sources, due to a large increase in uncertainty.

74En (Engleman 1974)

For transitions where the same assignment was given with multiple frequencies the ones with higher given intensity was taken. Blended lines with multiple assignments from different vibronic bands were given all assignments. 3 transitions ((0,0) R2(10) was decreased by 1 cm^{-1}, (0,0) R1(14) decreased by 1 cm^{-1}, and (0,0) P1(16) increased by 0.4 cm^{-1}) were shifted in order to become self consistent.

77DiWo (Dixon & Woods 1977)

Averaged of hyperfine splitting for ‘method 1’ in paper. Uncertainty taken as average difference between the methods.

89FuAlDa (Furio et al. 1989)

The uncertainty of the B $^2\Sigma^+$-X $^2\Sigma^+$ band was kept at 0.05 cm^{-1} as the reported relativity uncertainty, however the B $^2\Sigma^+$-A $^2\Pi$ band was increased to 0.1 cm^{-1} to ensure self-consistency.

94ItKaKu (Ito et al. 1994)

For the transitions from the B $^2\Sigma^+$-X $^2\Sigma^+$ (11-11) band where the same assignment was given to two frequencies the most intense (reported as ‘main’ in the paper) transition was included and others were not considered.

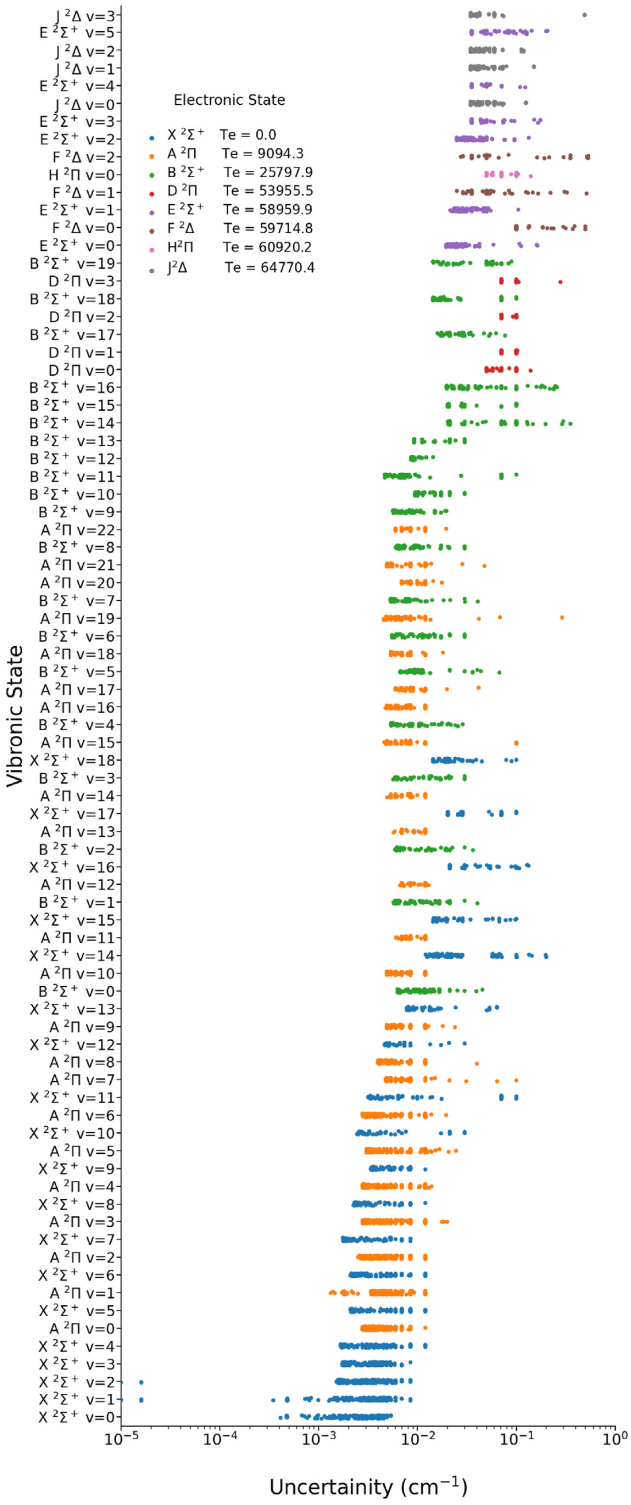

Figure 7. The spread of uncertainties for each vibronic state. The colours represent the electronic states that belong to each vibronic state, and the T_e of the electronic states are included in the legend.

04HoCiSp (Horká et al. 2004)

Reported quantum number given as J, however it is reported as an integer, and since J is half-integer for CN, we have taken the reported J as N, and determined J via the reported F quantum number.

Table 7. Summary of experimentally derived MARVEL energy levels, including uncertainties and data sources, for higher electronic states of CN. No is the number of energy levels in that vibronic state.

v	J range	E-range (cm^{-1})	No	Mean/max	Sources
$D^2\Pi$					
0	0.5–27.5	53955.5–54888.1	51	0.07/0.14	55DoRo
1	3.5–21.5	54954.7–55517.2	35	0.08/0.103	55DoRo
2	1.5–22.5	55917.5–56480.2	42	0.076/0.1	55DoRo
3	2.5–18.5	56869.4–57243.6	32	0.085/0.28	55DoRo
$E^2\Sigma^+$					
0	0.5–32.5	58959.9–60520.9	65	0.034/0.164	56Ca, 70Lu
1	0.5–42.5	60631.3–63280.0	85	0.034/0.105	56Ca, 70Lu
2	0.5–38.5	62285.0–64447.4	77	0.04/0.133	70Lu
3	0.5–42.5	63917.3–66529.9	85	0.047/0.175	70Lu
4	1.5–32.5	65529.3–67038.0	62	0.045/0.123	70Lu
5	0.5–37.5	67088.5–69082.0	75	0.061/0.207	70Lu
$F^2\Delta$					
0	2.5–32.5	59714.8–61112.9	58	0.142/0.5	55DoRo
1	1.5–16.5	60870.1–61314.8	54	0.076/0.514	71Lu
2	1.5–16.5	62058.8–62496.4	51	0.114/0.537	71Lu
$H^2\Pi$					
0	1.5–17.5	60920.2–61410.5	61	0.073/0.14	55DoRo
$J^2\Delta$					
0	1.5–28.5	64770.4–65816.3	102	0.045/0.126	56Ca
1	1.5–27.5	65856.6–66843.1	104	0.045/0.151	56Ca
2	1.5–30.5	66932.0–68186.6	114	0.045/0.119	56Ca
3	2.5–21.5	67984.8–68536.0	66	0.059/0.492	56Ca

05HuCaDa (Hübner et al. 2005)

Reported quantum number given as J, however it is reported as an integer, and since J is half-integer for CN, we have taken the reported J as N, and determined J via the reported F quantum number.

06RaDaWa (Ram et al. 2006)

Uncertainty was taken as experimental resolution. 26 transitions were removed for substantially larger uncertainties.

08CiSeKu (Civiš et al. 2008)

Uncertainty was taken as experimental resolution.

10RaWaBe (Ram et al. 2010)

Paper uses the F quantum number for A $^2\Pi$ state, with $F_1 \rightarrow \Omega = 1/2$ and $F_2 \rightarrow \Omega = 3/2$. As A $^2\Pi$ is an inverted Π state we have converted their use of F quantum number to explicit Ω. 12 transitions were removed for substantially larger uncertainties.

4 MARVEL EMPIRICAL ENERGY LEVELS FOR CN

4.1 Spectroscopic networks

The MARVEL process generates SN of interconnected energy levels connected by the input transition data. For the transition data used in this paper 134 SNs were generated with the main SN containing 7779 energy levels spanning 8 electronic states and 74 vibronic states. The other SNs are relatively small and composed of unconnected high

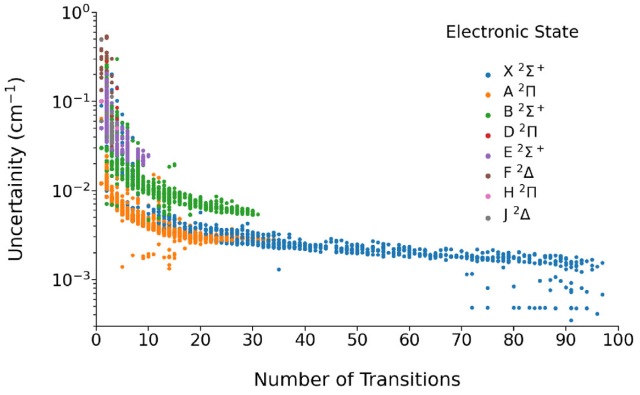

Figure 8. The relationship between the uncertainty of each energy level with the number of experimental transitions that contribute to it.

rotational transitions. The exception to this is four SNs that contain between 70 and 80 energy levels from the vibronic states; X $^2\Sigma^+$ (v = 15), X $^2\Sigma^+$ (v = 17), X $^2\Sigma^+$ (v = 18), B $^2\Sigma^+$ (v = 15), B $^2\Sigma^+$ (v = 18), and B $^2\Sigma^+$ (v = 19). These four mid-sized SNs were joined to the main SN using the 'Magic Number' technique. Joining these networks was accomplished by by adding four artificial transitions to the input file to join the ground state of X $^2\Sigma^+$to the J = 0.5 and 1.5 states of the X $^2\Sigma^+$v = 15 state. The frequency of these transitions was estimated by a combination of the energies in the main SN and data from the MOLLIST line list, with an uncertainty of 0.5 cm^{-1}. This brings the main SN up to 8083 energy levels from 80 vibronic states. An extract of the output file is included in Table 5, with the whole output file included in the SI. The rest of the SNs have less than 16 energy levels and no further analysis on these SNs were done.

The main SN is visualized in Fig. 4, by plotting the states as nodes and transitions as edges between them. Fig. 4 is broken up into the electronic bands (Fig. 4a), vibronic bands (Fig. 4b), and all rovibronic transitions in Fig. 4(c). Each electronic state is uniquely coloured, as labelled in Fig. 4(a) and this colour scheme flows through the vibronic and rovibronic levels as well. In Fig. 4(a), we can see that the A $^2\Pi$ state is the most connected to the other electronic states due to its Π symmetry. The interconnectivity of the lowest three electronic states gives rise to the clustering that is seen in Figs 4(b) and (c). This interconnectivity in Figs 4(b) and (c) also highlights how an upper state can decay into various different lower states. From the vibronic SN (Fig. 4b), we can see the extension of the higher vibrational B $^2\Sigma^+$-X $^2\Sigma^+$ bands from the bulk of the connected states. The rovibronic SN figure (Fig. 4c) is created from only the main SN of the CN data, with the unconnected isolated rovibronic states excluded for clarity. The high vibrational B $^2\Sigma^+$-X $^2\Sigma^+$ bands are much more apparent in Fig. 4(c) as the other rovibronic states become more connected and drawn towards the centre collection.

Since there are no observed transitions that involve the quartet states in CN they are not in any of the SNs. If there were observed transitions, they would only join the main SN through spin forbidden transitions, otherwise making a unique SN of their own.

4.2 Energy levels

All 221 spin-vibronic states are shown as unique lines in Fig. 5 as a function of the total angular momentum quantum number, J. The visibly smooth quadratic lines show no issues with 8083 empirical energy levels of the main SN. Fig. 5 also shows the range of J for the vibronic states, where low vibrational states in the ground X $^2\Sigma^+$ and A $^2\Pi$ electronic states have significantly higher rotational energy levels.

The distribution of the empirical uncertainties for each electronic state is shown in Fig. 6, which allows the median (shown as the flat line inside the largest box) to be visualized alongside increasingly smaller boxes as the distribution thins. Outliers are shown individually. Fig. 6 demonstrates the consistently increased uncertainties for higher electronic states, which are about an order of magnitude above the ground electronic state.

Delving deeper into the vibronic states for CN allows us to examine vibrational levels that have higher uncertainties. Table 6 breaks down the vibronic states for each of the lower electronic states, including: the J range, energy range, number of energy levels, mean and maximum empirical uncertainty, and the sources that contributed to the vibronic state. The X $^2\Sigma^+$ state is very well studied, especially at low vibration, as demonstrated by the large number of sources that contribute to the determination of the energy levels, as well as the small uncertainties. The low vibrational states of the A $^2\Pi$ and B $^2\Sigma^+$ states are fairly well characterized, but we see fewer sources as we increase the vibrational quantum number. The largest mean uncertainty of the lower electronic states is 0.073 cm^{-1} from B $^2\Sigma^+$ (v = 14). This state is well known to be perturbed by the A $^2\Pi$ (v = 30) vibronic state. Several of the known perturbed vibronic states can be seen to have an increased uncertainty spread in Fig. 7. While there is a general upward trend of uncertainties across vibronic states, the interaction of states can also be seen in the spread of uncertainties. The well-known near degeneracy of the X $^2\Sigma^+$(v = 11) and A $^2\Pi$(v = 7) can be seen through this lens, as well as the high vibrational X $^2\Sigma^+$and B $^2\Sigma^+$states. Many of the high vibrational B $^2\Sigma^+$ states are perturbed by high vibronic A $^2\Pi$ states not seen in this compilation, as well as the 'dark' quartet states. One example of this the B $^2\Sigma^+$ (v = 11) state that is thought to be perturbed by the a $^4\Sigma^+$ state (Coxon et al. 1975; Ozaki et al. 1983b), which has relatively low and clustered uncertainty, with a minimum of 0.005 cm^{-1} but has several energy levels with increased uncertainties of up to 0.1 cm^{-1}.

The higher electronic states have much fewer vibronic states observed. These vibronic states are given the same breakdown as the lower states in Table 7. All of these energy levels are only determined from one or two sources. The lack of experimental observation of these bands is highlighted in the F $^2\Delta$ state which has the highest average and mean uncertainties across all vibronic states.

The MARVEL process determines the uncertainties of each energy level based on the transitions that include that level. Fig. 8 demonstrates how the uncertainties of the transitions (shown in Fig. 3) propagate through to the uncertainties of the energy levels (see Figs 6 and 7). The uncertainty of the energy level is approximately an order of magnitude smaller than the uncertainties of the transitions involving those electronic states. Fig. 8 shows the uncertainty of the energy level as a function of the number of transitions that were involved in determining that energy level. The uncertainty of the energy levels decreases with an increase in the number of transitions, as expected. Thus, we can see that a larger number of experimental assignments allow for smaller uncertainties in the MARVEL procedure and thus a better understanding of the energy levels. The need for high-resolution assignments would only further benefit the understanding of energy levels in CN, especially of perturbed or higher electronic states, for which there are fewer data sources available.

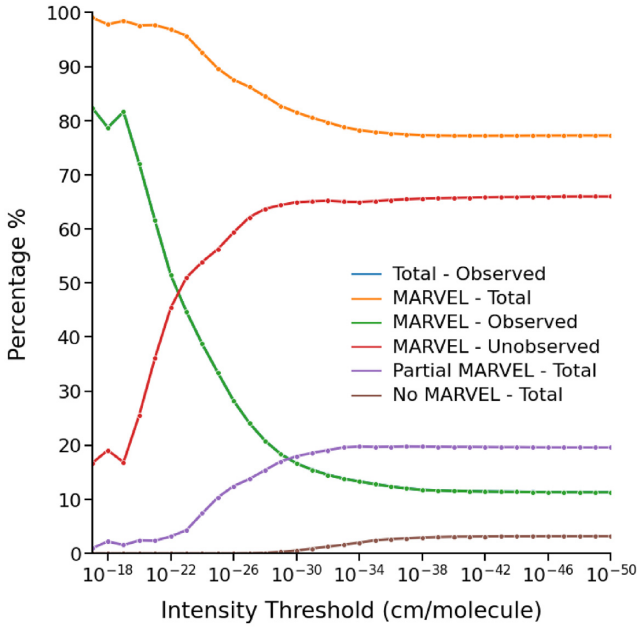

Figure 9. The percentage of transitions with degrees of MARVEL-ization across intensity calculated at 1000 K. The transitions with upper and lower energy levels that have been MARVEL-ized have also been split into observed and unobserved – according to the MOLLIST SI. The blue line indicating the Total — Observed (Observed in the MOLLIST SI) is indistinguishable from the MARVEL — Observed green line.

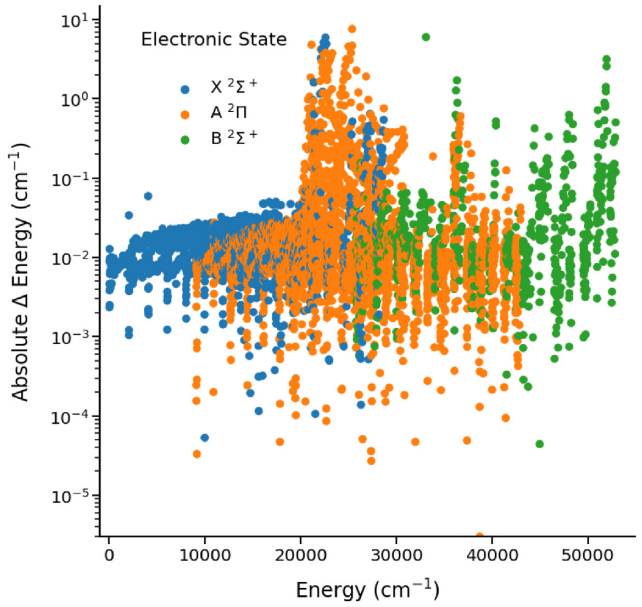

Figure 10. A comparison of the absolute energy difference (MARVEL — MOLLIST) of the 6122 energy levels from the MOLLIST data and the MARVEL procedure. Note the log scale of the *y*-axis.

5 UTILIZING MARVEL DATA TO IMPROVE THE MOLLIST CN LINE LIST

Currently, the most complete line list for CN is from MOLLIST (Brooke et al. 2014; Bernath 2020) created using the traditional method, that is, using spectroscopic constants fitted to experimental data. The sources of data used are a subset of those considered in this MARVEL compilation, specifically 91DaBrAb, 92PrBeFr, 92PrBe, 04HoCiSp, 05HuCaDa, 06RaDaWa, and 10RaWaBe. There are two versions of this CN line list currently available:

Original format, includes observed frequencies: contains only lower energy levels and transition frequencies. 11.3 per cent of the predicted frequencies are replaced with directly observed transition frequencies.

ExoMol formatted with predicted energies: the ExoMol format (Wang, Tennyson & Yurchenko 2020) calculates transition frequencies from energy levels rather than storing frequencies separately, ensuring self-consistency but reducing the quality of the line list frequencies for high-resolution applications. These energy levels are based solely on the predicted frequencies, that is, the spectroscopic constants.

Here, we produce a superior CN line list, the MARVELized MOLLIST line list, by using the ExoMol formatted version of the original MOLLIST line list, but replacing the predicted energy levels with the MARVEL experimentally derived energy levels where available; 6122 of the 7696 energy levels, that is, 79.5 per cent, are replaced. By propagating these improved energies through to the 195 112 transitions, we not only recover the 22 044 observed transitions but accurately predict an additional 128 751 transitions entirely from MARVEL energies, thus substantially improving the quality of the line list, especially for high-resolution studies. The updated ExoMol format 12C-14N__Mollist-Marvelized.states file is included in the SI, and is compatible with the 12C-14N__Mollist.trans file on the ExoMol website.

At 2000 K, MARVEL energy levels alone recover all but 0.000026 per cent of the partition function, while, even at 5000 and 7000 K, 98.2 per cent and 95.2 per cent of the partition function is recovered.

The spectral coverage of this new MARVELized MOLLIST CN line list is characterized in Fig. 9, which illustrates the source of transition frequency data as a function of minimum transition intensity at 1000 K. 81.6 per cent of strong transitions (intensities greater than 10^{-18} cm molecule^{-1}) have been directly observed, while an additional 16.8 per cent of transitions are unobserved but have frequencies determined completely from MARVEL energies. Of all of the transitions observed in the MOLLIST data set 99.9 per cent of them are matched with MARVEL data for both upper and lower energy levels, this is highlighted in Fig. 9 as the green line completely overlays the total observed transitions (blue line) along all intensities. As we consider weaker transitions, the proportion of directly observed transitions decreases, but the proportion of unobserved but fully MARVEL-ized transitions increases, keeping the number of transitions whose frequency is directly and completely determined by MARVEL energies above 77 per cent even when considering all MOLLIST transitions. The figure also details two other categories – partial MARVEL-ized transitions for which either the upper or lower state is a MARVEL energy but the other is predicted and No MARVEL transitions for which both upper and lower state energies are predicted from spectroscopic constants. These two groups contribute very few strong to moderate intensity transitions and are thus errors in the precise frequency of these transitions are unlikely to be important for cross-correlation of high-resolution spectra.

It is worthwhile to compare the predicted energy levels from the MOLLIST spectroscopic constants to the MARVEL energy levels in order to better understand the challenges of the traditional model approach. Fig. 10 shows the energy differences of the 6122 spin-

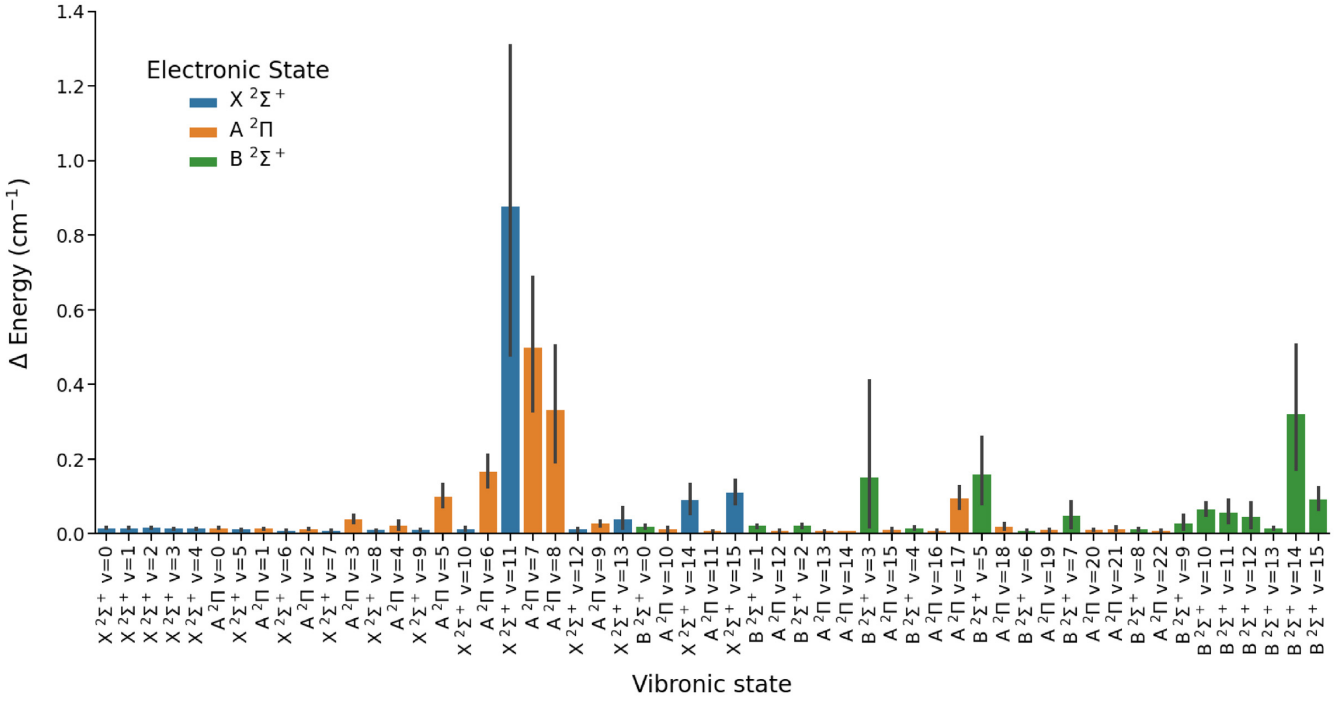

Figure 11. The average deviation between the MOLLIST and MARVEL vibronic energy levels, including standard deviation.

rovibronic energy levels that were matched in both data sets. The log scale is used here to highlight the majority of transitions that have an absolute deviation between the two data sets of less than 0.05 cm^{-1} (90th percentile). 20.8 per cent of the MARVEL–MOLLIST energy deviations are within the uncertainty of the MARVEL energy levels, with 71.9 per cent of the other deviations within an order of magnitude of the MARVEL uncertainties.

It is well known that spectroscopic constant fits struggle near perturbations and our results confirm this. Fig. 11 shows a bar plot of average absolute deviation of the vibronic states, including the standard deviation. While most vibronic states match very closely between MOLLIST and the empirical energy levels from MARVEL, this figure clearly identifies the outliers. These outliers are explored further in Fig. 12 which plots J versus change in energy for these vibronic states. This figure shows the systematic deviation between the spectroscopic constant fit and the experimentally derived energy levels as a function of J that is characteristic of perturbations (Ozaki et al. 1983a; Ito et al. 1994). Our results show the effects of strong known perturbations due to crossing of states occur between:

(i) A $^2\Pi$ ($v = 5$) and X $^2\Sigma^+$($v = 9$) at high J (Kotlar et al. 1980).
(ii) A $^2\Pi$ ($v = 6$) and X $^2\Sigma^+$($v = 10$) at high J (Kotlar et al. 1980).
(iii) A $^2\Pi$($v = 7$) and X $^2\Sigma^+$($v = 11$) states for J around 12.5 and 27.5 (Fallon, Vanderslice & Cloney 1962; Kotlar et al. 1980; Furio et al. 1989; Dagdigian et al. 1993; Ram et al. 2010).
(iv) A $^2\Pi$($v = 8$) collisional transfer with X $^2\Sigma^+$($v = 12$) (Furio et al. 1989).
(v) B $^2\Sigma^+$($v = 0$) crosses with X $^2\Sigma^+$($v = 14$) around $J = 29.5$ (Kotlar et al. 1980).
(vi) B $^2\Sigma^+$($v = 5$) and A $^2\Pi_{1/2}$ ($v = 17$) states for J between 8.5 and 12.5 (Jihua, Ali & Dagdigian 1986; Ram et al. 2010).
(vii) B $^2\Sigma^+$($v = 10$) perturbed by A $^2\Pi$ ($v = 24$) (Ozaki et al. 1983a, b).
(viii) B $^2\Sigma^+$($v = 11$) is perturbed by A $^2\Pi$ ($v = 26$) (Ito et al. 1994, 1984) and by a $^4\Sigma^+$ (Ozaki et al. 1983b; Coxon et al. 1975).
(ix) B $^2\Sigma^+$($v = 14$) is perturbed by A $^2\Pi$ ($v = 30$) (Ito et al. 1994; Ozaki et al. 1983b) and by b $^4\Pi$ (Ito et al. 1984) or a $^4\Sigma^+$ (Ozaki et al. 1983b).
(x) B $^2\Sigma^+$($v = 15$) is perturbed by A $^2\Pi$ ($v = 31$) (Ito et al. 1994).

It is worth noting that these highly perturbed energy levels are very likely to have high sensitivity to variation in the proton-to-electron mass ratio. Low-frequency transitions involving the A $^2\Pi$ ($v = 5-8$) states and the nearby X $^2\Sigma^+$ ($v = 8-11$) states are likely to have high sensitivity, though of course the lower state population and thus the transition intensities will be very low. The $\Delta = -4$ transitions, for example, X $^2\Sigma^+$ ($v = 11$) to A $^2\Pi$ ($v = 7$), are likely to be most sensitive, but their intensities are not predicted by MOLLIST. The $\Delta = -3$ transitions observed experimentally in Earth-based laboratories by 08CiSeKu (Civiš et al. 2008) at 6500 K have frequencies 1905.8–3117.2 cm^{-1}. MOLLIST predicts Einstein A coefficients of 6468 A $^2\Pi$-X $^2\Sigma^+$ $\Delta = -3$ transitions, but the high initial state energy means that the predicted intensities of these transitions is maximized at 3.0×10^{-28} cm molecule^{-1} at 1000 K (too small for realistic astrophysical study) rising to 5.5×10^{-21} cm molecule^{-1} at 7000 K. The higher temperatures definitely give rise to more realistically observable lines and we know that, due to its high dissociation energy, astrophysical CN can exist at high temperatures and has been found in stars (Briley & Smith 1993) and our Sun's sunspots (McKellar 1951).

6 CONCLUSION

Within this paper, we have collated all available sources of high-resolution rotationally resolved experimental transition assignments and determined empirical energy levels with reliable uncertainties for the CN radical through the MARVEL procedure. From 22 sources, 40 333 transitions were collated from 9 different electronic and 204

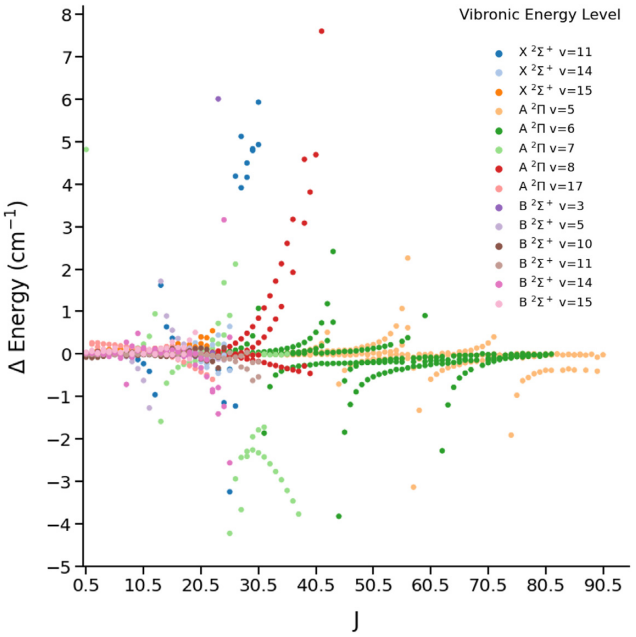

Figure 12. The energy deviations of the vibronic states along J, where the mean absolute deviation is greater than 0.05 cm^{-1}.

vibronic bands to generate 8083 energy levels spanning 8 electronic and 80 vibronic states. The relative lack of observed data of the higher electronic bands is evident.

The current line list for CN from MOLLIST has been updated with the empirical energy levels from the MARVEL analysis. 78.4 per cent of the energy levels have been replaced with MARVEL energies, recovering all but 0.0026 per cent of the partition function up to 2000 K. The MOLLIST transitions data have been MARVEL-ized with 77.3 per cent of all transitions being fully determined by experimentally derived MARVEL energy levels, compared to 11.3 per cent of directly observed transitions used in the MOLLIST line list. Of the strong transitions (intensities greater than 10^{-18} cm molecule^{-1}) 98.5 per cent have frequencies determined completely from MARVEL energies. The deviations between the MARVEL and MOLLIST energies arise in rovibronic levels with known perturbations, as expected.

The complexity of the CN radical, and the several near degenerate energy levels, shows promise for CN to be a possible molecular probe to test the variation of the proton-to-electron mass ratio. This will require a full spectroscopic model, which will be available in a future publication.

ACKNOWLEDGEMENTS

This research was undertaken with the assistance of resources from the National Computational Infrastructure (NCI Australia), an NCRIS enabled capability supported by the Australian Government.

The authors declare no conflicts of interest.

DATA AVAILABILITY STATEMENT

The data underlying this article are available in the article and in its online Supporting Information. These include the following files;

(i) README_CN.pdf – explanation of the files within the SI
(ii) 12C-14N_MARVEL.txt – the final MARVEL transitions file
(iii) 12C-14N_MARVEL.energies – the final MARVEL energies file
(iv) 12C-14N__Mollist-Marvelized.states – the updated states file for the MOLLIST line list, in ExoMol format (to be used with .trans file from the ExoMol website)
(v) SI.pdf – expanded analysis tables.

REFERENCES

Ajitha D., Hirao K., 2001, Chem. Phys. Lett., 347, 121
Bauschlicher Charles W. J., Langhoff S. R., Taylor P. R., 1988, ApJ, 332, 531
Beckman J., Carretero C., Vazdekis A., 2008, Astrophys. Space Sci., 277, 371
Bernath P. F., 2020, J. Quant. Spectr. Radiat. Transf., 240, 106687
Briley M. M., Smith G. H., 1993, PASP, 105, 1260
Brooke J. S. A., Ram R. S., Western C. M., Li G., Schwenke D. W., Bernath P. F., 2014, ApJS, 210, 23
Carroll P., 1956, Can. J. Phys., 34, 83
Cerny D., Bacis R., Guelachvili G., Roux F., 1978, J. Mol. Spectr., 73, 154
Civiš S., Šedivcová-Uhlíková T., Kubelík P., Kawaguchi K., 2008, J. Mol. Spectr., 250, 20
Colin R., Bernath P. F., 2012, J. Mol. Spectr., 273, 30
Colin R., Bernath P. F., 2014, J. Mol. Spectr., 302, 34
Coxon J. A., Ramsay D. A., Setser D. W., 1975, Can. J. Phys., 53, 1587
Császár A. G., Furtenbacher T., 2011, J. Mol. Spectr., 266, 99
Dagdigian P. J., Patel-Misra D., Berning A., Werner H. J., Alexander M. H., 1993, J. Chem. Phys., 98, 8580
Davis S. P., Brault J. W., Abrams M. C., Rao M. L. P., 1991, J. Opt. Soc. Am. B, 8, 198
Dixon T. A., Woods R. C., 1977, J. Chem. Phys., 67, 3956
Douglas A. E., Routly P. M., 1955, ApJS, 1, 295
Duric N., Erman P., Larsson M., 1978, Phys. Scr., 18, 39
Engleman R., 1974, J. Mol. Spectr., 49, 106
Fallon R. J., Vanderslice J. T., Cloney R. D., 1962, J. Chem. Phys., 37, 1097
Ferus M., Kubelík P., Knížek A., Pastorek A., Sutherland J., Civiš S., 2017, Nat. Sci. Rep., 7, 6275
Fray N., Bénilan Y., Cottin H., Gazeau M. C., Crovisier J., 2005, Planet. Space Sci., 53, 1243
Furio N., Ali A., Dagdigian P. J., Werner H. J., 1989, J. Mol. Spectr., 134, 199
Furtenbacher T., Császár A. G., 2012, J. Quant. Spectr. Radiat. Transf., 113, 929
Furtenbacher T., Császár A. G., Tennyson J., 2007, J. Mol. Spectr., 245, 115
Furtenbacher T., Szidarovszky T., Mátyus E., Fábri C., Császár A. G., 2013a, J. Chem. Theor. Comput., 9, 5471
Furtenbacher T., Szidarovszky T., Fábri C., Császár A. G., 2013b, Phys. Chem. Chem. Phys., 15, 10181
Furtenbacher T., Árendás P., Mellau G., Császár A. G., 2014, Sci. Rep., 4, 1
Furtenbacher T., Szabó I., Császár A. G., Bernath P. F., Yurchenko S. N., Tennyson J., 2016, ApJS, 224, 44
Furtenbacher T., Horváth M., Koller D., Sólyom P., Balogh A., Balogh I., Császár A. G., 2019, J. Phys. Chem. Ref. Data, 48, 023101
Gans B., Boyé-Péronne S., Garcia G. A., Röder A., Schleier D., Halvick P., Loison J. C., 2017, J. Phys. Chem. Lett., 8, 4038
Gorbal M. R., Savadatti M. I., 1981, Pramana, 16, 327
Gorbal M. R., Savadatti M. I., 1982, Chem. Rev., 82, 527
Hamano S. et al., 2019, ApJ, 881, 143
Hause M. L., Hall G. E., Sears T. J., 2009, J. Mol. Spectr., 253, 122
Henkel C., Mauersberger R., Schilke P., 1988, A&A, 201, 23
Horká V., Civiš S., Špirko V., Kawaguchi K., 2004, Collect. Czech. Chem. Commun., 69, 73
Hübner M., Castillo M., Davies P. B., Ropeke J., 2005, Spectrochim. Acta – Part A: Mol. Biomol. Spectr., 61, 57
Irwin T. A. R., Dalby F. W., 1965, Can. J. Phys., 43, 1766
Ito H., Ozaki Y., Nagata T., Kondow T., Kuchitsu K., 1984, Can. J. Phys., 62, 1586
Ito H., Ozaki Y., Suzuki K., Kondow T., Kuchitsu K., 1987, Chem. Phys. Lett., 139, 581

Ito H., Ozaki Y., Suzuki K., Kondow T., Kuchitsu K., 1988, J. Mol. Spectr., 127, 143
Ito H., Kazama A., Kuchitsu K., 1994, J. Mol. Struct., 324, 29
Jenkins F. A., 1928, Phys. Rev., 31, 539
Jenkins F. A., Roots Y. K., Mulliken R. S., 1932, Phys. Rev., 39, 193
Jihua G., Ali A., Dagdigian P. J., 1986, J. Chem. Phys., 85, 7098
Johnstone D., Boonman A. M., Van Dishoeck E. F., 2003, A&A, 412, 157
, Juncher D., Jørgensen U. G., Helling C., 608, 2017, A&A, A70
Kotlar A. J., Field R. W., Steinfeld J. I., Coxon J. A., 1980, J. Mol. Spectr., 80, 86
Kulik H. J., Steeves A. H., Field R. W., 2009, J. Mol. Spectr., 258, 6
Larsen S. S., Brodie J. P., Strader J., 2017, A&A, 601, 1
Leach S., 2012, MNRAS, 421, 1325
Leblanc F. J., 1968, CN J. Chem. Phys., 48, 403
Liu Y., Duan C., Liu H., Gao H., Guo Y., Liu X., Lin J., 2001, J. Mol. Spectr., 205, 16
Lutz B. L., 1970, Can. J. Phys., 48, 1192
Lutz B. L., 1971a, ApJ, 163, 131
Lutz B. L., 1971b, ApJ, 164, 213
McElroy D., Walsh C., Markwick A. J., Cordiner M. A., Smith K., Millar T. J., 2013, A&AS, 550, 1
McGuire B. A., 2018, ApJS, 239, 17
McKellar A., 1940, Astron. Soc. Pac., 52, 187
McKellar A., 1951, Leaflet Astron. Soc. Pac., 6, 114
McKemmish L. K. et al., 2017, ApJS, 228, 15
McKemmish L. K. et al., 2018, ApJ, 867, 33
McKemmish L. K., Masseron T., Hoeijmakers H. J., Pérez-Mesa V., Grimm S. L., Yurchenko S. N., Tennyson J., 2019, MNRAS, 488, 2836
Ozaki Y., Nagata T., Suzuki K., Kondow T., Kuchitsu K., 1983a, Chem. Phys., 80, 73
Ozaki Y., Ito H., Suzuki K., Kondow T., Kuchitsu K., 1983b, Chem. Phys., 80, 85
Peng Z.-M., Ding Y.-J., Xiao-Dong Z., Yang Q.-S., Jiang Z.-L., 2011, Chin. Phys. Lett., 28, 044703
Phillips J. G., Chun M. L., 1973, Stat. Field Theor., 180, 607
Poletto G., Rigutti M., 1965, Il Nuovo Cimento Ser. 10, 39, 519
Pradhan A. D., Partridge H., Bauschlicher C. W., 1994, J. Chem. Phys., 101, 3857
Prasad C. V., Bernath P. F., 1992, J. Mol. Spectr., 156, 327
Prasad C. V., Bernath P. F., Frum C., Engleman R., 1992, J. Mol. Spectr., 151, 459
Qin Z., Zhao J. M., Liu L. H., 2017, J. Quant. Spectr. Radiat. Transf., 202, 286
Ram R. S., Bernath P. F., 2012, J. Mol. Spectr., 274, 22
Ram R. S., Davis S. P., Wallace L., Engleman R., Appadoo D. R. T., Bernath P. F., 2006, J. Mol. Spectr., 237, 225
Ram R. S., Wallace L., Bernath P. F., 2010, J. Mol. Spectr., 263, 82
Rehfuss B. D., Suh M. H., Miller T. A., Bondybey V. E., 1992, J. Mol. Spectr., 151, 437
Riffel R., Pastoriza M. G., Rodríguez-Ardila A., Maraston C., 2007, ApJ, 659, L103
Ritchey A. M., Federman S. R., Lambert D. L., 2015, ApJ, 804, L3
Schmidt M. R., Krełowski J., Weselak T., Galazutdinov G. A., 2013, MNRAS, 431, 1795
Schoonveld L., 1972, J. Quant. Spectr. Radiat.Transf., 12, 1139
Schoonveld L. H., 1973, J. Chem. Phys., 58, 403
Schoonyeld L., Sundaram S., 1979, ApJS, 41, 669
Shi D., Liu H., Zhang X., Sun J., Zhu Z., Liu Y., 2010, J. Mol. Struct.: THEOCHEM, 956, 10
Shi D., Li W., Sun J., Zhu Z., 2011, J. Quant. Spectr. Radiat. Transf., 112, 2335
Shinnaka Y. et al., 2017, AJ, 154, 45
Smith V. V. et al., 2013, ApJ, 765, 16
Sneden C., Lucatello S., Ram R. S., Brooke J. S. A., Bernath P., 2014, ApJS, 214, 26
Sneden C., Cowan J. J., Kobayashi C., Pignatari M., Lawler J. E., Den Hartog E. A., Wood M. P., 2016, ApJ, 817, 53
Soltani A., Moradi A. V., Bahari M., Masoodi A., Shojaee S., 2013, Phys. B: Cond. Matter, 430, 20
Syme A. M., Mousley A., Cunningham M., McKemmish L. K., 2019, Aust. J. Chem. , 73, 743
Tennyson J., Lodi L., McKemmish L. K., Yurchenko S. N., 2016, Journal of Physics B: Atomic, Molecular and Optical Physics, 49, 102001
Wang Y., Tennyson J., Yurchenko S. N., 2020, Atoms, 8, 7
Wasowicz T. J., Kivimäki A., Coreno M., Zubek M., 2014, J. Phys. B: Atom. Mol. Opt. Phys., 47, 1
Weinberg J. M., Fishburne E. S., Narahari Rao K., 1967, J. Mol. Spectr., 22, 406
Woon D. E., 2006, Chem. Phys., 331, 67
Xun J., Deng J., He R., 2019, Chem. Phys. Lett., 733, 136695
Yin Y., Shi D., Sun J., Zhu Z., 2018, ApJS, 235, 120
Yurchenko S. N., Szabó I., Pyatenko E., Tennyson J., 2018, MNRAS, 480, 3397

SUPPORTING INFORMATION

Supplementary data are available at *MNRAS* online.

suppl_data

Please note: Oxford University Press is not responsible for the content or functionality of any supporting materials supplied by the authors. Any queries (other than missing material) should be directed to the corresponding author for the article.

This paper has been typeset from a TEX/LATEX file prepared by the author.